Available online at www.sciencedirect.com
ScienceDirect
Journal of Power Sources 168 (2007) 200–210
JOURNAL OF POWER SOURCES
www.elsevier.com/locate/jpowsour

Experimental evaluation and mathematical modeling of a direct alkaline fuel cell

A. Verma [1], S. Basu *

Department of Chemical Engineering, Indian Institute of Technology Delhi, New Delhi 110016, India

Received 25 December 2006; received in revised form 23 February 2007; accepted 26 February 2007
Available online 7 March 2007

Abstract

The performance of a direct alkaline fuel cell (AFC) is studied separately using methanol, ethanol and sodium borohydride as fuel. Potassium hydroxide solution was used as an electrolyte. Pt-black and manganese dioxide catalyst were used to prepare the anode and cathode electrodes. Ni mesh was used as current collector. The direct alkaline fuel cell was constructed with the prepared anode and cathode electrodes and Ni mesh. The current density–cell voltage characteristics of the fuel cell were determined by varying load and at different experimental conditions, e.g., electrolyte concentration, fuel concentration and temperature. The fuel cell performance increases initially with the increase in electrolyte (KOH) concentration and then decreases with further increase of the same. The cell performance increases initially and then no appreciable improvement noticed with the increase in fuel concentration. The performance of the fuel cell increases with increase in temperature in general with the exception to $NaBH_4$ alkaline fuel cell. A mathematical model for the direct alkaline fuel cell is developed based on reaction mechanism available in the literature to predict the cell voltage at a given current density. The model takes into account activation, ohmic, concentration overpotentials and other losses. The model prediction is in fair agreement with the experimental data on current–voltage characteristics and captures the influence of different experimental conditions on current–voltage characteristics.

Keywords: Direct alkaline fuel cell; Over potentials; Cell performance; Fuel cell modeling

1. Introduction

Alkaline fuel cell (AFC) was the first fuel cell technology used in many practical applications like Apollo space missions and automobiles [1,2]. The development of AFC technology had reached its peak in the beginning of 1980s [3] but its further development was stopped due to many technical, commercial and safety issues. In last few years, the interest on AFC increased due to more favorable oxygen reduction [4,5] and fuel oxidation reactions [6] in alkaline condition. Apart from these, the cost, simplicity, efficiency and the possibility of use of non-noble metal catalyst [3,7] compared to other low temperature fuel cell technology have given an impetus to the AFC research. The detailed comparisons of AFC and polymer electrolyte membrane fuel cell (PEMFC) technologies based on hydrogen fuel is given by McLean et al. [8]. Though, the hydrogen as a fuel has many advantages but the certain obstacles have led to look into possibility of direct use of hydrogen-rich liquid and solid fuels in fuel cells. Some of the obstacles associated with the use of hydrogen as fuel are the generation of pure hydrogen in large quantity at a lower cost comparable to gasoline cost, on board storage of hydrogen (low density), low power output per unit weight of the fuel cell and fuel processor and safety issues [2]. The investigators are working on direct feeding of hydrogen rich fuels, e.g., alcohols, ethers, N_2H_4, NH_3, and $NaBH_4$ into the alkaline fuel cells [9–14]. These fuel cells are operated at a low temperature (20–60 °C) and produce low power density. Thus, direct alkaline fuel cell is suitable for use as power source to portable electronic equipments.

Among the fuels, methanol is an attractive liquid fuel because it is relatively cheap, readily available, solubility in aqueous electrolytes, easily stored and handled. Energy density of methanol is 6 kWh kg^{-1} (5 kWh L^{-1}). Ideally, the electrochemical oxidation of methanol produces six electrons per molecule of methanol.

* Corresponding author. Tel.: +91 11 26591035; fax: +91 11 26581120.
E-mail addresses: anil.verma@iitg.ernet.in (A. Verma), sbasu@chemical.iitd.ac.in (S. Basu).
[1] Present address: Department of Chemical Engineering, Indian Institute of Technology Guwahati, Assam 781039, India.

0378-7753/$ – see front matter © 2007 Elsevier B.V. All rights reserved.
doi:10.1016/j.jpowsour.2007.02.069

Nomenclature

A	area of the electrode (m^2)
C	concentration of oxygen at cathode catalyst surface ($kmol\,m^{-3}$)
C_E	concentration of ethanol ($mol\,L^{-1}$)
C_M	concentration of methanol ($mol\,L^{-1}$)
C_o	concentration of oxygen in air ($kmol\,m^{-3}$)
c_{OH}	concentration of KOH ($g\,cc^{-1}$)
C_{OH}	concentration of KOH ($mol\,L^{-1}$)
C_{SB}	concentration of sodium borohydride ($mol\,L^{-1}$)
D_{eff}	effective diffusivity of oxygen from electrode composite ($m^2\,s^{-1}$)
$D_{o,air}$	diffusivity of oxygen from air ($m^2\,s^{-1}$)
E	open circuit voltage (V)
E_{cell}	cell voltage at any load (V)
F	Faraday constant ($C\,mol^{-1}$)
J	current density ($A\,m^{-2}$)
j_0	exchange current density ($A\,m^{-2}$)
k_i	rate constant of forward reaction in Eqs. (16)–(18), (23)–(25) and (27)–(29), i = 1–9 ($L\,m^{-2}\,s^{-1}$)
K_E	constant for ethanol oxidation in Eq. (26) ($C\,L^3\,mol^{-2}\,m^{-2}\,s^{-1}$)
K_M	constant for methanol oxidation in Eq. (21) ($C\,L^3\,mol^{-2}\,m^{-2}\,s^{-1}$)
K_{SB}	constant for sodium borohydride oxidation in Eq. (30) ($C\,L^3\,mol^{-2}\,m^{-2}\,s^{-1}$)
K_i	adsorption-desorption equilibrium constant in Eq. (22) (i = 1, 2), 26 (i = 4, 5) and 30 (i = 7, 8) ($L\,mol^{-1}$)
k_i'	rate constant of backward reaction in Eqs. (16) and (17), (23)–(24) and (27)–(28), i = 1–8 ($i \neq 3$, 6) ($mol\,m^{-2}\,s^{-1}$)
k_i^0	standard rate constant in Eqs. (19), (26) and (30) (i = 3, 6 and 9) ($mol\,m^{-2}\,s^{-1}$)
L	parameter in Eq. (A.1.1) (V)
M	constant, $M = A\delta C_o / nF\varepsilon^{3/2} D_{o,air}$
n	number of electrons
N	parameter in Eq. (A.1.1) (dimensionless)
N_o	oxygen molar flux ($kmol\,m^{-2}\,s^{-1}$)
r_i	rate of the reaction in Eqs. (16)–(18), (23)–(25) and (27)–(29) (i = 1–9) ($mol\,m^{-2}\,s^{-1}$)
R	gas constant ($J\,mol^{-1}\,K^{-1}$)
R_{oh}, R'_{oh}	area specific resistance ($\Omega\,cm^2$)
T	temperature (K)
T_1	temperature (°C)

Greek letters

α	transfer coefficient for the oxidation of different fuels (methanol, ethanol and sodium borohydride)
β	transfer coefficient for oxygen reduction
δ	thickness of cathode (m)
ε	porosity of cathode (dimensionless)
η	overpotential (V)
η_{ac}	activation overpotential (V)
η_{conc}	concentration overpotential (V)
η_{FL}	undesired losses (V)
η_{oh}	ohmic overpotential (V)
θ_{CH_3CO}	fractional coverage of adsorbed CH_3CO species (dimensionless)
θ_{HBO_2}	fractional coverage of adsorbed HBO_2 species (dimensionless)
θ_{HCO}	fractional coverage of adsorbed HCO species (dimensionless)
θ_{OH}	fractional coverage of adsorbed OH species (dimensionless)

However, methanol has disadvantages such as high toxicity, low boiling point (65 °C) and not a primary fuel. Therefore other alcohols, particularly those derived from biomass resources are considered, as they are renewable in nature. Ethanol is one of the potential fuels as it is easily produced in large quantity by fermentation of biomass. The energy density of ethanol is about 7.44 kWh kg^{-1} (5.9 kWh L^{-1}) and it produces 12 electrons per molecule of electro-oxidation of ethanol. It is a non-toxic chemical and its boiling point is relatively higher compared to that of methanol. Ethanol and the higher alcohols have the drawback that their C–C bond rupture is difficult in the presence of noble metal catalyst in the temperature range of 25–90 °C [15]. Among solids fuels, sodium borohydride is gaining attention because it contains 10.6-wt.% hydrogen and 7 kWh g^{-1} of energy density, which is much more than the most of the hydrogen storage alloys. The electro-oxidation reaction products of $NaBH_4$ are environmentally safe. Although hydrogen as a fuel is easily obtained from the hydrolysis reaction of borohydrides, the direct anodic oxidation of borohydride provides more negative potential than that of hydrogen gas. From the above discussion, it is clear that methanol, ethanol and sodium borohydride has excellent potential as fuel for direct alkaline fuel cell.

In the present investigation a direct alkaline fuel cell is constructed and its performance in the form of current–voltage characteristics is determined at different experimental conditions, e.g., fuel and electrolyte concentrations and temperature. The modeling of direct alkaline fuel cell based on methanol or ethanol or sodium borohydride as fuel is not reported in the open literature as far as the knowledge of the investigators. A mathematical model on direct alkaline fuel cell is developed and the model predictions are compared with the experimental data on current–voltage characteristics at different operating conditions.

2. Experimental

2.1. Materials

The catalyst used for the preparation of anode, Pt-black, was procured from Johnson Matthey Inc., UK. Manganese dioxide used in the cathode was procured from E. Merck. The carbon paper (484C-1, Lydall, USA) was used as a substrate for catalyst particles. Nafion® (SE-5112) and Teflon® disper-

sions used as adhesives were obtained from DuPont, USA. Pure nickel screen (mesh 10) was used as current collector because it is highly resistive to alkaline condition and good electrical conductor. Analytical grade of methanol, ethanol and sodium borohydride were obtained from E. Merck. Potassium hydroxide was obtained from Qualigen Fine Chemicals, India. Freshly prepared distilled water was used in all the experiments.

2.2. Electrode preparation

The anode electrode was prepared by dispersing the required quantity of catalyst powder in Nafion® solution for 30 min using an ultrasonic water bath to the prepare catalyst slurry. The catalyst slurry was spread on a carbon paper in the form of continuous wet film. It is then dried in an oven for 30 min at 80 °C. The catalyzed carbon paper was stuck on to the nickel mesh using Teflon® dispersion. The prepared electrode was pressed at a pressure of 50 kg cm^{-2} and temperature of 120 °C for 5 min to obtain the composite structure of the electrode. The area of the working electrode was 10 cm^2. Finally, the composite was heated at 573 K for 4 h to obtain final form of the anode electrode. The cathode electrode was prepared in a similar manner using MnO_2 as catalyst to obtain the composite structure. An additional carbon paper was stuck on to air-side of the electrode with the help of Teflon dispersion. Finally, a Teflon film was stuck on to the carbon paper to obtain the final form of the cathode electrode. Thus the cathode consist of four layers, i.e., the catalyst layer on the carbon paper, nickel mesh, the second layer of carbon paper and the Teflon layer. The porous Teflon layer on air side of the cathode helps in restricting KOH electrolyte transport to the air side and at the same time allows diffusion of oxygen from air to catalyst layer.

2.3. Experimental set-up

The schematic diagram of the experimental set-up is shown in Fig. 1. The prepared anode was placed at the bottom of a glass beaker. A hollow cylinder with cathode attached to one of the open ends, was placed inside the beaker. Two wires connected to anode and cathode were acted as terminals. The space between anode and cathode was filled with mixture of electrolyte and fuel solution. The fuel cell was kept in a water bath (not shown in Fig. 1) to keep the temperature of the fuel cell constant. The fuel-electrolyte and exhausted-fuel storage tanks were connected to inlet and outlet of the fuel cell by flexible tubes through peristaltic pumps. A magnetic stirrer was used to maintain uniformity of fuel-electrolyte mixture. To protect the anode from the stirrer, the anode was shielded with the help of a perforated plastic support. The terminals of the cell were connected to the digital multimeter (Sanwa PC5000, Japan) through variable load. The oxygen present in air acted as oxidant. The detail of the experimental set-up and procedure are given in Verma et al. [11,12].

2.4. Method

Half-cell analyses of Pt-black anode and MnO_2 cathode were conducted using cyclic voltammetry. The optimize conditions

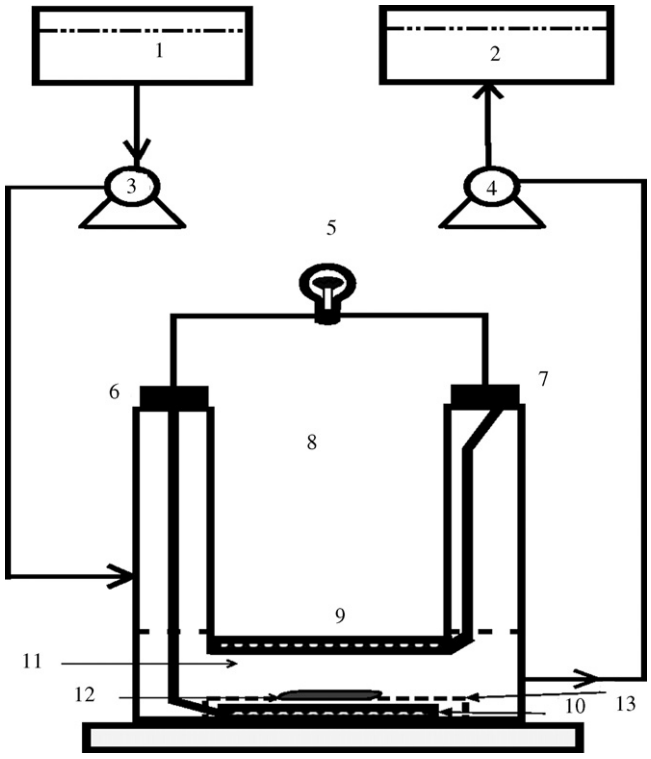

Fig. 1. Schematic diagram of the direct alkaline fuel cell. (1) Fuel-electrolyte storage; (2) exhausted-fuel-electrolyte storage; (3 and 4) peristaltic pumps; (5) load; (6) anode terminal; (7) cathode terminal; (8) air; (9) cathode electrode; (10) anode electrode; (11) fuel and electrolyte mixture; (12) magnetic stirrer; and (13) anode shield.

of fuel and electrolyte concentrations were determined for maximum current density. The alkaline fuel cell constructed was fed with mixture of given concentrations of fuel (methanol or ethanol or sodium borohydride) and electrolyte (KOH) solution from the storage tank at the rate of 1 mL min^{-1}. The fuel and electrolyte solution was maintained up to a certain level such that the one side of the cathode was in contact with electrolyte while the other side exposed to air. The solution was continuously stirred with a magnetic stirrer, which was located on the perforated anode shield. The heat of the reaction is carried out of the fuel cell by the un-reacted fuel, products and electrolyte mixture. The open circuit voltage (OCV) and the short circuit current were measured with the help of a multimeter. The voltage and corresponding current was measured at different loads to obtain *j–v* (current density–cell voltage) characteristic curve. The steady-state values of voltage and current were noted in all the experiments and the reproducibility of data is checked. The influence of different experimental conditions, e.g., electrolyte concentration, fuel concentration and temperature on fuel cell performance were noted. The area resistance of the fuel cell was measured by the current interruption technique using a potentiostat.

3. Model development

Electrical energy is obtained from a fuel cell when a current is drawn, but at the same time, cell voltage drops due to vari-

ous irreversible losses. The performance of fuel cell is generally reduced due to the loss of some electrical energy to drive the oxidation and reduction reaction at the anode and cathode, which is known as activation overpotential, and ohmic resistance of the electrolyte, electrolyte–electrode interface and the electrodes. Further, the loss occurs due to the mass transfer resistance experienced by fuel and oxidant to reach the anode and cathode, which is known as concentration overpotential. These losses are denoted by η_{ac} as the activation overpotential, η_{oh} as the ohmic overpotential and η_{conc} as the concentration overpotential. Thus, the cell voltage, E_{cell}, is written as,

$$E_{cell} = E - (\eta_{ac} + \eta_{oh} + \eta_{conc}) \quad (1)$$

where E is the open circuit voltage. Before the expressions for each overpotential losses are derived, the mechanisms of electro oxidation and reduction reaction are discussed.

3.1. Mechanism of electro-oxidation and electro-reduction

The electro-oxidation reaction mechanism of methanol as proposed by Tripković et al. [16] is used to model the activation overpotential. Tripković et al. [16] suggested a dual-path reaction mechanism (Eq. (2) during electro-oxidation of alcohols (methanol, ethanol, *n*-propanol and *n*-butanol) in an alkaline solution.

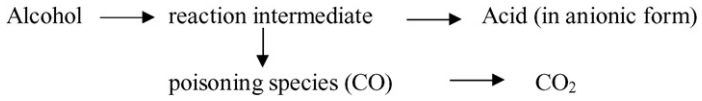

(2a)

(2b)

The end product of methanol electro-oxidation reaction is formic acid. However, in alkaline medium formic acid exists in the form of formate ion. Apart from formic acid a small quantity of carbon dioxide is also formed [16] and it is neglected in the model development. In the literature, the report on identification of the products formed during oxidation of methanol in alkaline solution is scanty. The path shown by Eq. (2a) is the main reaction path and assumes the formation of reactive intermediates, weakly bonded to the surface [17].

$$CH_3OH \Leftrightarrow HCO_{ad} + 3H^+ + 3e^- \xrightarrow{+3OH^-} 3H_2O \quad (3)$$

$$OH^- \Leftrightarrow OH_{ad} + e^- \quad (4)$$

$$HCO_{ad} + OH_{ad} \rightarrow HCOOH \quad (5)$$

Eq. (3) is a dehydrogenation process involving several steps and may be written as follows [18,19]:

$$CH_3OH \xrightarrow{-H(H^+ + e^-)} CH_3O_{ad} \xrightarrow{-H(H^+ + e^-)} CH_2O_{ad} \xrightarrow{-H(H^+ + e^-)} CHO_{ad} \quad (6)$$

Only a few literatures are available on the ethanol electro-oxidation. The C–C bond breaking for the complete oxidation of ethanol impedes the process of ethanol electro-oxidation. There is no electrocatalyst, which enables complete ethanol oxidation in the temperatures range of 30–90 °C [15,20,21]. Acetic acid forms as a final product of ethanol electro-oxidation. A small quantity of carbon dioxide generated as reported by Tripković et al. [16] and Tarasevich et al. [21] is neglected in the model development. The reaction mechanism for ethanol electro-oxidation is similar to that of methanol electro-oxidation [16], which is given by,

$$C_2H_5OH \Leftrightarrow CH_3CO_{ad} + 3H^+ + 3e^- \xrightarrow{+3OH^-} 3H_2O \quad (7)$$

$$OH^- \Leftrightarrow OH_{ad} + e^- \quad (8)$$

$$CH_3CO_{ad} + OH_{ad} \rightarrow CH_3COOH \quad (9)$$

Morris et al. [22] reviewed the electro-oxidation of boron compounds and mentioned that the anodic oxidation of BH_4^- in alkaline medium on platinum electrode occurs via ionization of hydrogen from the parent ion (BH_4^-) and from the first hydrolysis product, BH_3OH^-, bound to the electrode surface. They pointed out similar mechanism of borohydride oxidation as that of methanol. Lee et al. [9] studied the characterization of an alkaline fuel cell that uses $NaBH_4$ as fuel. The reaction mechanism suggested by them is given below:

$$BH_4^- \Leftrightarrow HBO_{2ad} + 5H_2O + 8e^- \quad (10)$$

$$OH^- \Leftrightarrow OH_{ad} + e^- \quad (11)$$

$$HBO_{2ad} + OH_{ad} + e^- \rightarrow BO^-_2 + H_2O \quad (12)$$

The reduction of oxygen in alkaline medium generally proceeds by either of the two pathways [23,24]. They are described below as direct oxygen reduction to OH^- ions, i.e., a four-electron pathway:

$$O_2 + 2H_2O + 4e^- \rightarrow 4OH^- \quad (13)$$

or, an oxygen reduction to HO_2^- ions, i.e., two electron pathway:

$$O_2 + H_2O + 2e^- \rightarrow HO^-_2 + OH^- \quad (14)$$

with subsequent reduction of peroxide ion to OH^- ions, i.e., two electron pathway:

$$HO^-_2 + H_2O + 2e^- \rightarrow 3OH^- \quad (15)$$

Eqs. (14) and (15) are collectively produce 2 + 2 electron mechanism [23]. The cyclic voltammmetry and oxygen consumption experiments have shown that the oxygen electro-reduction reaction follows four-electron transfer mechanism [11].

3.2. Activation overpotential

Activation overpotential is directly related to the electrochemical reaction kinetics since the reaction propagates at the

rate demanded by the specific load. At no load condition, oxidation–reduction reactions reach equilibrium at the electrodes. The current density related to electron transfer in such oxidation–reduction reactions is known as exchange current. Many investigators [3–6,25] studied the cathode reaction in alkaline condition and reported that the oxygen reduction kinetics is more favorable at cathode as compared to the oxidation of fuel at anode. Thus, it is assumed that the activation overpotential at cathode is less significant compared to that at anode. In the following sections, the expressions for activation overpotentials are derived for different fuels.

3.2.1. Methanol

The electro-oxidation reaction mechanism of methanol (Eqs. (3)–(5)) as proposed by Tripković et al. [16] is used to model the activation overpotential. Eqs. (3) and (4) are assumed much faster than the overall reaction rate-determining step (Eq. (5)). In our model development the reaction order with respect to methanol concentration is 1.0, whereas reaction order with respect to OH^- is taken as 0.5 [18]. The rate expressions for Eqs. (3)–(5) are given below:

$$r_1 = k_1 C_M - k_1' \theta_{HCO} \tag{16}$$

$$r_2 = k_2 C_{OH}^{0.5} - k_2' \theta_{OH} \tag{17}$$

$$r_3 = k_3 \theta_{HCO} \theta_{OH}^{0.5} \tag{18}$$

In Eqs. (16)–(18), k_1, k_2 and k_3 are the rate constants for the forward reactions (Eqs. (3–5)) and k_1' and k_2' are the rate constants for the backward reactions (Eqs. (3) and (4)). The expression for k_3 is given by [26]:

$$k_3 = k_3^0 \exp\left(\frac{\alpha n F \eta_{ac}}{RT}\right) \tag{19}$$

where α is the transfer coefficient, which is defined as the proportion of the electrical energy used for changing the rate of electrochemical reaction (Eq. (5)). Its value depends on the nature of the reaction and the electrode material and its value must be between 0 and 1.0. The value for α in the case of methanol oxidation is found as 0.22. Wang et al. [25] used α value of 0.24 for a similar reaction. n, the number of electrons transferred during oxidation of methanol, is 4. Here, k_3^0 is the standard rate constant, F the Faraday constant, T the temperature and R is the universal gas constant. The concentration of methanol and OH^- are represented by C_M and C_{OH} (mol L^{-1}), respectively. r_i (i = 1–3) is the rate of reaction and θ_i (i = OH, HCO) is the fractional coverage defined as the ratio of number of adsorbed species to the total number of surface sites of the catalyst. At equilibrium, r_1 and r_2 is equated to zero and by solving the Eqs. (16)–(18) it follows:

$$r_3 = k_3 K_1 K_2 C_M C_{OH}^{0.5} \tag{20}$$

where K_1 ($=k_1/k_1'$) and K_2 ($=k_2/k_2'$) are adsorption–desorption equilibrium constants correspond to Eqs. (3) and (4), respectively.Also, the net rate of the electrode reaction is governed by the rate-determining step hence it is expressed as:

$$r_3 = \frac{j}{nF}, \tag{21}$$

where j is the current density. On solving Eqs. (19)–(21), the relation between activation overpotential and current density for methanol is given by,

$$\eta_{ac} = \left(\frac{RT}{\alpha n F}\right) \ln\left(\frac{j C_M^{-1} C_{OH}^{-0.5}}{K_M}\right), \tag{22}$$

where K_M ($=nFk_3^0 K_1 K_2$) is a constant for methanol oxidation. The appropriate values for k_3^0, K_1 and K_2 are required to estimate K_M.

3.2.2. Ethanol

The reaction mechanism (Eqs. (7)–(9)) proposed by Tripković et al. [16] is used to model the activation overpotential for ethanol electro-oxidation. The reaction order with respect to ethanol concentration is taken as 1.0, whereas reaction order with respect to OH^- is taken as 0.5 [21]. The corresponding rate expressions for Eqs. (7)–(9) are given below:

$$r_4 = k_4 C_E - k_4' \theta_{CH_3CO} \tag{23}$$

$$r_5 = k_5 C_{OH}^{0.5} - k_5' \theta_{OH} \tag{24}$$

$$r_6 = k_6 \theta_{CH_3CO} \theta_{OH}^{0.5} \tag{25}$$

where k_4, k_5 and k_6 are the rate constants of the forward reactions (Eqs. (7)–(9)), k_4' and k_5' are the rate constants of the backward reactions (Eqs. (7) and (8)). Following similar method that carried out in the case of methanol and using α value of 0.3 and n = 4, the relation between activation overpotential and current density for ethanol is given by,

$$\eta_{ac} = \left(\frac{RT}{\alpha n F}\right) \ln\left(\frac{j C_E^{-1} C_{OH}^{-0.5}}{K_E}\right), \tag{26}$$

where K_E ($=nFk_6^0 K_4 K_5$) is a constant for ethanol oxidation.

3.2.3. Sodium borohydride

The reaction mechanism (Eqs. (10)–(12)) suggested by Morris et al. [22] is taken into consideration and the corresponding rate expressions are given below:

$$r_7 = k_7 C_{SB} - k_7' \theta_{HBO_2} \tag{27}$$

$$r_8 = k_8 C_{OH}^{0.5} - k_8' \theta_{OH} \tag{28}$$

$$r_9 = k_9 \theta_{HBO_2} \theta_{OH}^{0.5} \tag{29}$$

where k_7, k_8 and k_9 are the rate constants of the forward reactions (Eqs. (10)–(12)), k_7' and k_8' are the rate constants of the backward reactions (Eqs. (10) and (11)). The order of the reaction with respect to borohydride is taken as 1.0 and 0.5 with respect to OH^- ion [22]. Using similar procedure as described before and taking α = 0.3 and n = 8, the relation between activation overpotential and current density for sodium borohydride

is given by,

$$\eta_{ac} = \left(\frac{RT}{\alpha n F}\right) \ln\left(\frac{j C_{SB}^{-1} C_{OH}^{-0.5}}{K_{SB}}\right), \quad (30)$$

where K_{SB} ($=nFk_9^0 K_7 K_8$) is a constant for sodium borohydride.

3.3. Ohmic overpotential

In modeling of ohmic overpotential, it is assumed that the ohmic drop in current collectors and electric connections is negligible and change in resistance of electrolyte due to the presence of fuel is insignificant. The first assumption is reasonable since modeling of single fuel cell is involved and stack is not considered. The second assumption implies that the ohmic losses are same for all the three fuels used. The ohmic losses are proportional to the current density and represented as:

$$\eta_{oh} = jR_{oh}, \quad (31)$$

where R_{oh} is the area specific resistance offered by electrolyte for ion transport. The variation of resistance with the KOH concentration is reported by Jo and Yi [27]. The expression for area specific resistance, R'_{oh}, at 25 °C is determined from the regression analyses of the experimental data on resistance and KOH concentration presented by Jo and Yi [27]. The expression for area specific resistance, R'_{oh}, at 25 °C is found out as follows:

$$R'_{oh} = 13.1737 - 90.336c_{OH} + 230.5735c_{OH}^2 - 81.07083c_{OH}^3 \quad (32)$$

It is well known that the resistance to ionic mobility decreases in the electrolyte solution with the increase in temperature. The final expression modified for area specific resistance in terms of KOH concentration and temperature is determined from the experimental data and is given by:

$$R_{oh} = R'_{oh} - 25.78 + 1.1875T_1 - 0.00625T_1^2, \quad (33)$$

where c_{OH} is the concentration of KOH in g cc^{-1}, T_1 the temperature in °C and R'_{oh} is the area specific resistance[2] in Ω cm^2.

3.4. Concentration overpotential

Normally, oxygen at the cathode of a fuel cell is supplied in the form of air. The oxygen consumption at cathode leads to the decrease in its partial pressure at the cathode. The extent of decrease in partial pressure will depend on the current drawn from the fuel cell. The decrease in partial pressure or concentration of oxygen results in concentration overpotential as the oxygen will not be replenished immediately at the cathode because of the mass transfer resistance. The similar phenomena occur in the anode compartment where the oxidation of fuel takes place and fuel concentration decreases. In the experimental set-up it is shown that the fuel and electrolyte mixture is well stirred. Thus, the effect of concentration overpotential at anode is reduced considerably and it is assumed to be insignificant compared to that at cathode. The schematic diagram of the cathode is shown in Fig. 2. It is seen in Fig. 2 that oxygen present in air has to diffuse through porous Teflon layer, gas diffusion layer, Ni-mesh and another gas diffusion layer to reach cathode catalyst (MnO_2) surface. In estimating the mass transfer resistance the thickness of the composite cathode made of gas diffusion layers and Teflon layer is considered. It is assumed that the Ni-mesh offers negligible resistance. It is further assumed that the concentration of oxygen at the interface of air and gas diffusion layer is C_o, i.e. the bulk concentration of oxygen in the air, while the concentration of oxygen at the catalyst layer is C. Under steady-state condition and from species conservation, the oxygen molar flux, N_o, is related to the current density, j, by:

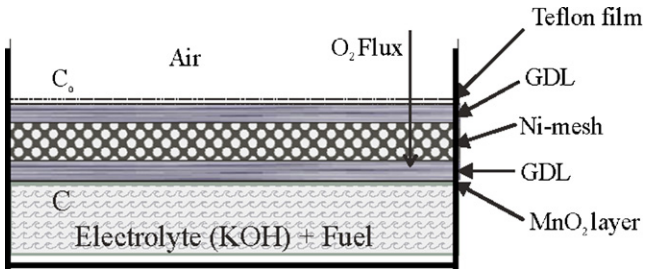

Fig. 2. Schematic diagram of cathode components.

$$N_o = \frac{j}{nF} \quad (34)$$

One-dimensional Fick's law in terms of the molar flux of oxygen is used to describe the transport of oxygen in the gas diffusion layer. It is given by,

$$N_o = -D_{eff}\frac{C_o - C}{\delta} \quad (35)$$

where δ is the thickness of electrode, D_{eff} is the effective diffusivity of the oxygen–nitrogen gas pair in the porous media with the porosity ε. D_{eff} is evaluated from the bulk diffusivity, $D_{O,air}$, using Bruggeman's correction [28]:

$$D_{eff} = \varepsilon^{3/2} D_{O,air} \quad (36)$$

The catalyst layer is regarded as a thin film located on the gas diffusion layer. The rate of the electrochemical reaction within the catalyst layer is described using Butler-Volmer equation [26]. It is then simplified in terms of oxygen concentration at the cathode catalyst layer as [24]:

$$j = j_0 \frac{C}{C_o} \exp\left(\frac{\beta n \eta_{conc} F}{RT}\right) \quad (37)$$

where β is the transfer coefficient and j_o is the exchange current density. The value of β varies from 0 to 1.0 and in the present case it is assumed as 0.3. The value of n depends on the stoicheometry of oxygen reduction reaction. Since cathode reaction ($O_2 + 2H_2O + 4e^- = 4OH^-$) is same for all the fuels,

[2] Note that unit of length is in cm because the original experimental data published by Jo and Yi [25] is in cm and the regression analyses expression is valid for the same unit. In our final calculation of ohmic loss, the length unit is converted to m.

i.e., methanol, ethanol and sodium borohydride, the value of n is 4. The exchange current density is given by [25]:

$$j_0 = 0.0422 \exp\left\{\frac{73200}{R}\left(\frac{1}{353} - \frac{1}{T_1}\right)\right\}, \quad (38)$$

where T_1 is temperature in °C. On solving Eqs. (34)–(37), the expression for concentration overpotential is given by,

$$\eta_{\text{conc}} = \frac{RT}{\alpha n F}\ln\left[\frac{J}{j_o(1 - jM)}\right] \quad (39)$$

where M is a constant as defined in Eq. (40) and A is the area of the electrode.

$$M = \frac{A\delta C_o}{nF\varepsilon^{3/2}D_{o.air}} \quad (40)$$

3.5. Model equations

In the model development, it is assumed that the direct alkaline fuel cell is operated at steady state and isothermal condition is prevailed. The final reaction for the direct methanol alkaline fuel cell is given by the adding two half-cell reactions taking place at anode (Eq. (3)–(5)) and cathode (Eq. (13)) and it is given by,

$$CH_3OH + O_2 \rightarrow HCOOH + H_2O \quad (41)$$

By incorporating the expressions for activation (Eq. (22)), ohmic (Eq. (33)) and concentration (Eq. (37)) overpotentials in equation (Eq. (1)), the final model equation is obtained for direct methanol alkaline fuel cell as,

$$E_{\text{cell}} = E - \left(\frac{RT}{\alpha n F}\right)\ln\left(\frac{jC_M^{-1}C_{OH}^{-0.5}}{K}\right) - jR_{\text{oh}} - \frac{RT}{\alpha n F}\ln\left(\frac{j}{j_o(1 - jM)}\right) \quad (42)$$

Similarly by adding the half-cell reactions of ethanol (Eq. (7)–(9) and sodium borohydride (Eq. (10)–(12)) to oxygen reduction reaction (Eq. (13)), the reactions for direct ethanol and borohydride alkaline fuel cells are given by,

$$C_2H_5OH + O_2 \rightarrow CH_3COOH + H_2O \quad (43)$$

$$BH_4^- + 2O_2 \rightarrow BO_2^- + 2H_2O \quad (44)$$

The model equations for ethanol and sodium borohydride are obtained from Eqs. (26), (33), (37) and (30), (33), (37), respectively. The model equation for direct ethanol alkaline fuel cell is given by:

$$E_{\text{cell}} = E - \left(\frac{RT}{\alpha n F}\right)\ln\left(\frac{jC_E^{-1}C_{OH}^{-0.5}}{K'}\right) - jR_{\text{oh}} - \frac{RT}{\alpha n F}\ln\left(\frac{j}{j_o(1 - jM)}\right) \quad (45)$$

The model equation for direct borohydride alkaline fuel cell is given by:

$$E_{\text{cell}} = E - \left(\frac{RT}{\alpha n F}\right)\ln\left(\frac{jC_{SB}^{-1}C_{OH}^{-0.5}}{K''}\right) - jR_{\text{oh}} - \frac{RT}{\alpha n F}\ln\left(\frac{j}{j_o(1 - jM}\right) \quad (46)$$

From the above equations (Eqs. (42), (45) and (46)), the operating voltage and current density at a given load of the direct alcohol or borohydride alkaline fuel cell is determined at the known rate constants and operating conditions, e.g., fuel concentration, electrolyte concentration and temperature.

4. Results and discussion

The experimental data on cell voltage and current density at different operating conditions are presented and compared with model predictions.

4.1. Electrolyte concentration

Fig. 3a–c shows the experimental data and model predictions on current density–cell voltage (j–v) characteristics at four different KOH concentrations for methanol, ethanol and sodium borohydride at 25 °C. It is seen in the figures that the cell voltage increases with the increase in KOH concentration in the range of 1–3 M and then it decreases with the further increase in KOH concentration. The reason for the decrease in voltage may be the less availability of methanol at the catalyst site with the increase in KOH concentration. The experimental data on j–v plot shown by symbols are predicted by the model as shown by the lines for different KOH concentrations. The model prediction in the region of concentration overpotential shows larger deviation compared to the regions of activation and ohmic overpotentials. It may be because of the assumption made in the model that the concentration overpotential at anode is negligible compared to that at cathode. The abrupt dip in the cell voltage at a higher current density is not predicted by the model because of the above assumption and perhaps due to undesired methanol oxidation at cathode at a high current density.

4.2. Fuel concentration

Fig. 4a–c shows current density–voltage characteristics, where the experimental data are shown by symbols and the model predictions are shown by lines, for four different fuel concentrations of methanol, ethanol and sodium borohydride, respectively. It is seen in the figures that the cell voltage increases with the increase in fuel concentration for a given value of current density. Although the cell performance increases initially but it does not increase proportionally with further increase in fuel concentration. The reasons may be because of the decrease in hydroxyl ion mobility with the increase in fuel concentration. Also, the active sites for hydroxyl ion adsorption might have been blocked by the fuel. Although 3 M alcohol concentra-

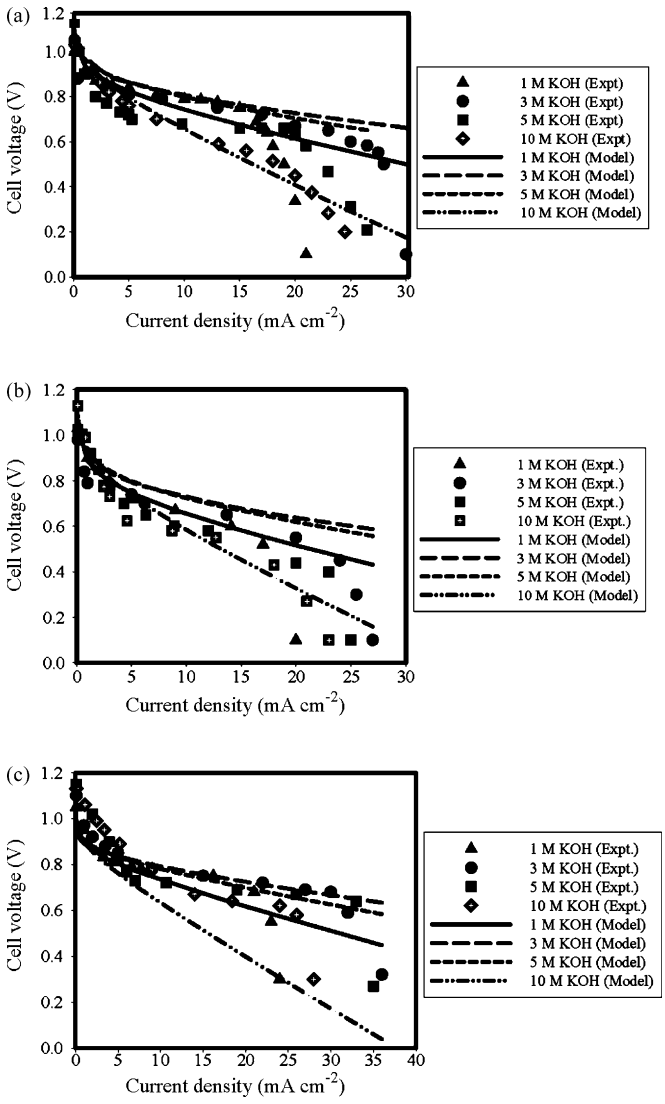

Fig. 3. Comparison of experimental data with model predictions pertaining to current–voltage characteristics for 2 M fuel at different electrolyte (KOH) concentrations ($T_1 = 25\,^{\circ}C$): (a) methanol (b) ethanol and (c) sodium borohydride.

tion generated slightly higher cell performance, the difference in performance between 3 and 2 M alcohol concentration is negligible. Subsequently, experiments were carried out at 2 M alcohol concentration to study the effect of temperature. The current density-cell voltage plots are somewhat predicted by the model for different fuel concentrations. The model overpredicts the experimental data in the region of higher current density, where concentration overpotential is dominant. The higher current density originates because of the lower load and consequently faster reaction kinetics expected at the anode and cathode. The sharp decrease in cell voltage value at a higher current density compared to that predicted by the model may be because of the oxidation of fuel at cathode at a higher fuel concentration, especially when system demands higher reaction kinetics at the electrodes.

4.3. Temperature

Fig. 5a–c shows the experimental data and model predictions on current density–voltage characteristics at three different operating temperatures for 3 M KOH and 2 M methanol, ethanol, sodium borohydride, respectively. It is seen in the figures that the cell voltage increases with the increase in temperature for a given value of current density. The performance increases with the increase in temperature because of decrease in activation overpotential, concentration overpotential and increase in ionic conductivity and mobility at a higher temperature. The performance of direct sodium borohydride alkaline fuel cell does not increase appreciably with the increase in temperature and in fact shows decreasing trend in current–voltage characteristics at 65 °C. The reason for this decrease may be because of hydrogen gas generation from sodium borohydride at higher temperature. The hydrogen gas generated escapes from the cell without reacting. The maximum power density of 24.3 and 14.5 mW cm^{-2} were obtained for methanol and ethanol at 65 °C while that for $NaBH_4$ was 22.5 mW cm^{-2} at 25 °C. The experimental data, shown by the symbols, are reasonably predicted by the model as shown by the lines except at a higher current density. The reason

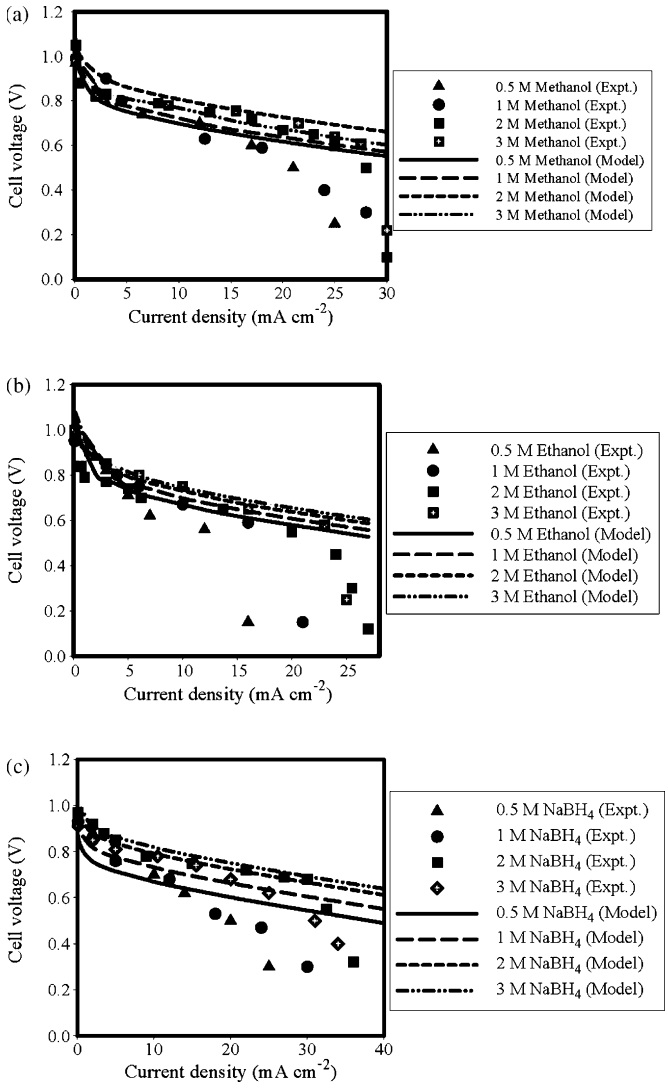

Fig. 4. Comparison of experimental data with model predictions pertaining to current–voltage characteristics at different fuel concentrations ($T_1 = 25\,^{\circ}C$; $C_{OH} = 3$ M): (a) methanol (b) ethanol and (c) sodium borohydride.

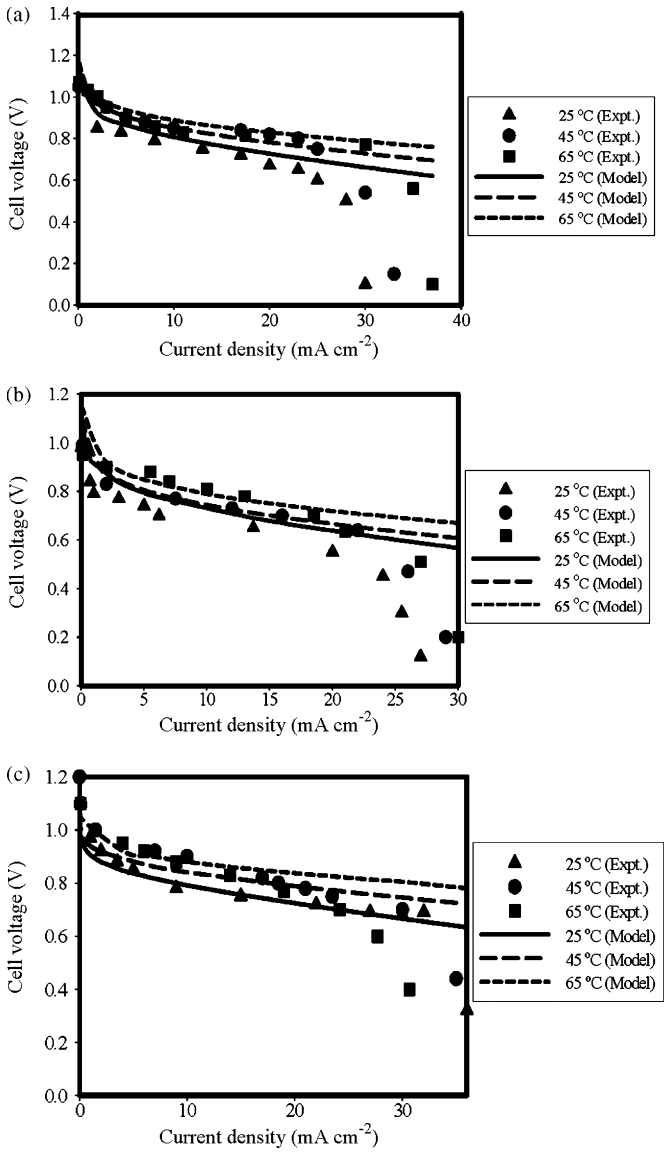

Fig. 5. Comparison of experimental data with model predictions pertaining to current–voltage characteristics for 2 M fuel at different temperatures (C_{OH} = 3 M): (a) methanol (b) ethanol and (c) sodium borohydride.

for overprediction of experimental data at a higher temperature is already discussed.

A consistent overprediction of experimental data by the model at a higher current density has led to the idea of addition of an excess concentration overpotential term to take into account of various undesired losses at the electrodes, e.g., oxidation of fuel at cathode and concentration overpotential at anode. The additional term used in the model is given in the appendix. Fig. 6a–c shows that the modified model predicts the experimental data well in the range of higher current density values for methanol and ethanol. Fig. 6a and b shows the prediction by the modified model for methanol at different KOH and fuel concentrations, respectively. Whereas, Fig. 6c shows the prediction by the modified model at different operating temperatures for direct ethanol alkaline fuel cell. It should be noted that source of error in modeling may be from the use of Eq. (1) in which overpotential terms are added in linear manner. Since kinetics of the reaction at anode and cathode depends on concentration, an integrated approach should be taken to account for all the losses. A consistent over prediction of the cell voltage at a higher current density may have resulted due to assumed linear behavior of the loss terms.

4.4. Model parameters

The parameters used in the model Eqs. (42), (45) and (46) for different fuels, e.g., methanol, ethanol and sodium borohydride are presented in Table 1. It is seen that the fitted value for the adsorption and desorption constants, K_1 and K_2 of Eq. (20) and the rate constant, k_3^0 (Eq. (19)), of the rate determining step is of the same order of magnitude to that found in literature for similar reaction involving methanol at 70 °C. The constant, K_E, for ethanol as listed in Table 1 is of the same order that for

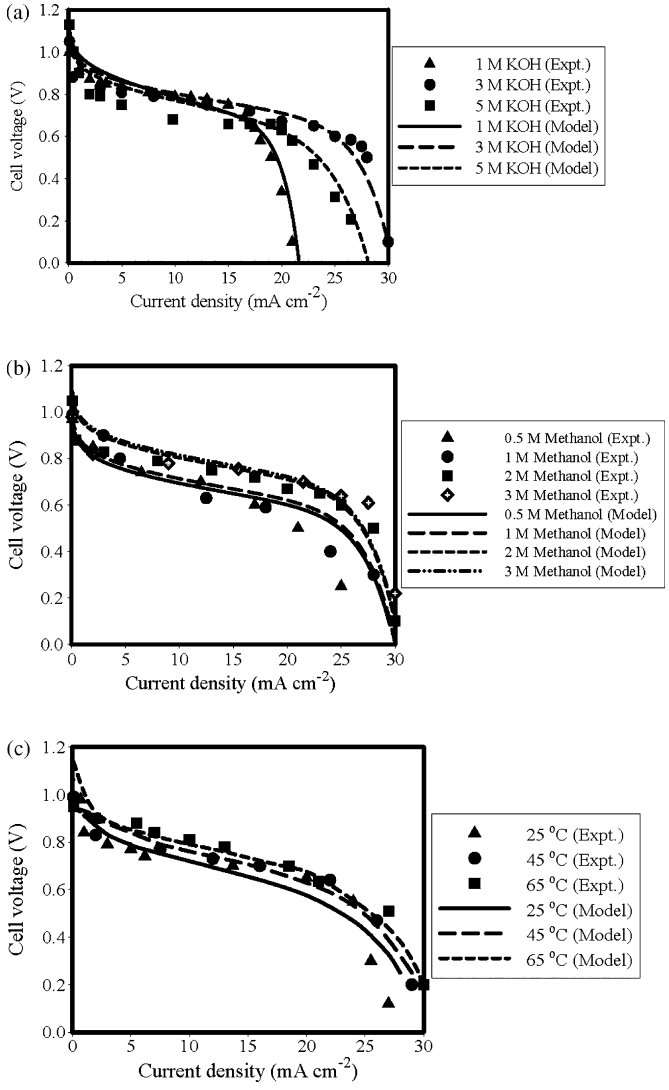

Fig. 6. Comparison of experimental data with predictions by the modified model pertaining to current–voltage characteristics (T_1 = 25 °C unless otherwise specified): (a) 2 M methanol at different KOH concentrations (b) 3 M KOH at different methanol concentrations (c) 2 M ethanol and 3 M KOH concentrations at different temperatures.

Table 1
Model Parameters

Parameter	Temperature	Unit	Present model value/literature value	Reference
K_1	65 °C	mol^{-1} L	1.0/1.0 (at 70 °C)	Sundmacher et al. [17]
K_2	65 °C	mol^{-1} L	0.01/0.01 (at 70 °C)	Sundmacher et al. [17]
k_3^0	65 °C	mol m^{-2} s^{-1}	0.155/0.01 (at 70 °C)	Sundmacher et al. [17]
K_M ($=nFK_1K_2k_3^0$)	25 °C	mol^{-1} L	3.0/not available	Sundmacher et al. [17]
	45 °C		5.0/not available	
	65 °C		6.0/38.6 (at 70 °C)	
K_E ($=nFK_4K_5k_6^0$)	25 °C	mol^{-1} L	1.0/not available	Not available
	45 °C		2.3/not available	
	65 °C		4.0/not available	
K_{SB} ($=nFK_7K_8k_9^0$)	25 °C	mol m^{-2} s^{-1}	0.001/not available	Not available
	45 °C		0.03/not available	
	65 °C		0.25/not available	
α		Dimensionless	0.22/0.24	Wang et al. [23]
α'		Dimensionless	0.3/0.5	Tarasevich et al. [19]
α''		Dimensionless	0.3/not available	Not available
β		Dimensionless	0.3/0.1–0.5	Larminie and Dicks [27]

methanol, K_M. It is expected that the rate constants of electrooxidation reaction and adsorption and desorption constants for two consecutive alcohols in the homologous series should be of the same order of magnitude. Since the rate constants for eletrooxidation and adsorption and desorption constants for ethanol and $NaBH_4$ on electrode surface are not reported in the literature, they are not compared in Table 1. The α values for different fuels and the β value used are within the comparable range as quoted in the different literatures [19,25,29].

5. Conclusions

The direct alkaline fuel cell constructed for the use of methanol, ethanol, sodium borohydride as fuel was tested and current–voltage characteristic curves were obtained at different experimental conditions, e.g., electrolyte concentration, fuel concentration and temperature. Pt-black was used as the anode catalyst and MnO_2 was used as the cathode catalyst. KOH solution was used as the electrolyte. The cell performance increases initially with the increase in electrolyte (KOH) concentration and then decreases with the further increase of the same. Initially, the cell performance increases with the increase in fuel concentration, but no appreciable increase in the performance is recorded at a higher fuel concentration. The performance of the fuel cell increases with increase in temperature in general with the exception to $NaBH_4$ alkaline fuel cell. A mathematical model for the prediction of voltage at a given current density of direct alkaline fuel cell is developed, by taking into account the losses due to activation, ohmic and concentration overpotentials. The activation overpotential term is formulated using reaction mechanisms proposed earlier in the half-cell studies. Ohmic overpotential is modeled based on conductivity of electrolyte solution (KOH) at different temperatures. The concentration overpotential is formulated using Fick's law and Butler-Volmer equation. The model reasonably predicts the experimental data on cell voltage and current density and captures the influence of electrolyte and fuel concentrations and temperature with the exception to data at a higher current density. Addition of an excess concentration overpotential term to the model equation further improves the model prediction for the given range of current density.

Acknowledgements

The authors gratefully acknowledge the financial support of the Ministry of New and Renewable Energy, India and Indian Institute of Technology Delhi for the above project.

Appendix A. Undesired losses at the electrodes

The direct alkaline fuel cell has suffered from minute losses at the electrodes in the range of high current density. These losses are concentration overpotential at anode and undesired fuel oxidation at cathode as stated earlier. An important observation in the modeling study is that the difference between model prediction and experimental data increases with the increase in the current density. At a higher current density, the fuel at the anode is used up at a faster rate not allowing to be replenished because of the mass transfer resistance. An excess loss term as a function of current density is added to the model equation to quantify the various losses [30]. This is given by,

$$\eta_{FL} = L \times \exp(N \times j) \quad \text{(A.1.1)}$$

where η_{FL} is the excess concentration overpotential, L and N are functions of the electrolyte concentration. L and N have been obtained empirically for the different fuels from experimental data. The constants L and N for methanol are found out by regression analyses as, $L = 1 \times 10^{-7} \times e^{1.45C_{OH}}$, $N = 0.0026C_{OH}^2 - 0.025C_{OH} + 0.0877$ and that for ethanol, $L = 9 \times 10^{-7} \times e^{2.3C_{OH}}$, $N = 0.0021C_{OH}^2 - 0.025C_{OH} + 0.0758$ and for sodium borohydride, $L = 2 \times 10^{-9} \times e^{1.15C_{OH}}$, $N = 0.0014C_{OH}^2 - 0.015C_{OH} + 0.079$. The regression coefficient is 0.985.

References

[1] L. Carrette, K.A. Friedrich, U. Stimming, Fuel Cells 1 (2001) 5–39.
[2] K. Kordesch, J. Gsellmann, M. Cifrain, S. Voss, V. Hacker, R. Aronson, C. Fabjan, T. Hejze, J. Daniel-Ivad, J. Power Sources 80 (1999) 190–197.
[3] M. Schulze, E. Gülzow, J. Power Sources 127 (2004) 252–263.
[4] T. Burchardt, P. Gouérec, E. Sanchez-Cortezon, Z. Karichev, J.H. Miners, Fuel 81 (2002) 2151–2155.
[5] E.H. Yu, K. Scott, J. Power Sources 137 (2004) 248–256.
[6] M.A.A. Rahim, R.M.A. Hameed, M.W. Khalil, J. Power Sources 134 (2004) 160–169.
[7] M. Cifrain, K. Kordesch, Hydrogen/oxygen (air) fuel cells with alkaline electrolytes, in: W. Vielstich, H.A. Gasteiger, A. Lamm (Eds.), Handbook of Fuel Cells—Fundamentals, Technology and Applications, vol. 1, John Wiley, 2003, pp. 267–280.
[8] G.F. McLean, T. Niet, S. Prince-Richard, N. Djilali, Int. J. Hydrogen Energy 27 (2002) 507–526.
[9] S. Lee, J. Kim, H. Lee, P. Lee, J. Lee, J. Electrochem. Soc. 149 (2002) A603–A606.
[10] G. Koscher, K. Kordesch, J. Power Sources 136 (2) (2004) 215–219.
[11] A. Verma, A.K. Jha, S. Basu, J. Power Sources 141 (2005) 30–34.
[12] A. Verma, A.K. Jha, S. Basu, J. Fuel Cell Sci. Technol. 2 (2005) 234–237.
[13] S. Basu (Ed.), Recent Trends in Fuel Cell Science and Technology, Springer/Anamaya, 2007.
[14] A. Verma, S. Basu, J. Power Sources 145 (2005) 282–285.
[15] C. Lamy, E.M. Belgsir, J.-M. Léger, J. Appl. Electrochem. 31 (2001) 799–809.
[16] A.V. Tripković, K.Dj. Popović, J.D. Lović, Electrochim. Acta 46 (2001) 3163–3173.
[17] E. Morallón, A. Rodes, J.L. Vázquez, J.M. Pérez, J. Electroanal. Chem. 391 (1995) 149–157.
[18] A.V. Tripković, K.Dj. Popović, J.D. Momčilović, D.M. Dražić, J. Electroanal. Chem. 418 (1996) 9–20.
[19] K. Sundmacher, T. Schultz, S. Zhou, K. Scott, M. Ginkel, E.D. Gilles, Chem. Eng. Sci. 56 (2001) 333–341.
[20] G.A. Camara, R.B. Lima, T. de Iwasita, Electrochem. Commun. 6 (2004) 812–815.
[21] M.R. Tarasevich, Z.R. Karichev, V.A. Bogdanovskaya, E.N. Lubnin, A.V. Kapustin, Electrochem. Commun. 7 (2005) 141–146.
[22] J.H. Morris, H.J. Gysling, D. Reed, Chem. Rev. 85 (1985) 51–76.
[23] J. Ortiz, M. Puelma, J.L. Gautier, J. Chil. Chem. Soc. 48 (2003) 67–71.
[24] J. Yang, J.J. Xu, Electrochem. Commun. 5 (2003) 306–311.
[25] Y. Wang, L. Li, L. Hu, L. Zhuang, J. Lu, B. Xu, Electrochem. Commun. 5 (2003) 662–666.
[26] A.J. Bard, L.R. Faulkner, Electrochemical methods: Fundamentals and Applications, second ed., John Wiley & Sons, 2001, pp. 226–260.
[27] J. Jo, S. Yi, J. Power Sources 84 (1999) 87–106.
[28] K.T. Jeng, S.F. Lee, G.F. Tsai, C.H. Wang, J. Power Sources 138 (2004) 41–50.
[29] J. Larminie, A. Dicks, Fuel Cell Systems Explained, second ed., John Wiley & Sons Ltd., 2003, pp. 48–53.
[30] H. Dohle, K. Wippermann, J. Power Sources 135 (2004) 152–164.